Journal of
Applied Crystallography

ISSN 0021-8898

Received 16 August 2006
Accepted 31 January 2007

Residual orientation in micro-injection molded parts

John Healy,[a]* Graham H. Edward[a] and Robert B. Knott[b]

[a]Department of Materials Engineering, Monash University, Australia, and [b]Bragg Institute, Australian Nuclear Science and Technology Organisation, Australia. Correspondence e-mail: john.healy@eng.monash.edu.au

The residual orientation following micro-injection molding of small rectangular plates with linear polyethylene has been examined using small-angle neutron scattering, and small- and wide-angle X-ray scattering. The effect of changing the molding conditions has been examined, and the residual chain orientation has been compared to the residual orientation of the crystallites as a function of position in the sample. This study has found that, for micromoldings, the orientation of the crystallites decreases with increasing injection speed and increasing mold thickness. The combined data suggest that the majority of the orientation present comes from oriented crystal growth rather than residual chain orientation.

1. Introduction

Injection molding is a commonly used fabrication technique for mass production using polymeric materials. The effects of the injection molding process on the microstructure and residual orientation of polymeric materials has been the subject of ongoing research for many years. The morphology of injection molded samples is strongly affected by the processing conditions and often has a complex layered structure due to the different shear and thermal histories of material through the part (Katti & Schultz, 1982). More recent research includes the examination of the microstructure of small molded parts produced through micro-injection molding (Ito *et al.*, 2005). These studies commonly use techniques such as infrared dichroism, nuclear magnetic resonance and optical birefringence to measure the average orientation of segments of the polymer chain and/or use X-ray scattering techniques to examine the crystalline orientation and morphology.

Previous studies have noted that oriented crystal structures can form in sheared melts that had largely relaxed prior to crystallization (Pople *et al.*, 1996). The aim of the present study is to examine the development of orientation in injection molded systems and compare the resultant orientation of the crystallites with the residual chain orientation. This study uses small-angle neutron scattering (SANS) to examine the orientation of the polymer chains and X-ray scattering to examine the orientation of the crystallites. The results from the SANS experiments examining the chain orientation at a molecular scale for micro-injection molded samples of polyethylene and polystyrene have been published previously (Healy *et al.*, 2004).

In both polymer systems, commercial polydisperse polymers were doped with a deuterated analogue with a narrow molecular weight distribution similar to the weight average molecular weight of the polydisperse matrix polymer. The polystyrene samples showed strong chain orientation that increased with decreasing mold thickness and decreased with increasing injection velocity.

In this SANS study, the modulus of the scattering vector, q, is defined as

$$q = (4\pi/\lambda)\sin(\theta), \qquad (1)$$

where 2θ is the angle between the incident and scattered radiation and λ is the wavelength of the incident radiation.

The polyethylene samples showed strong orientation in the intermediate-q region ($qR_g > 1$) that followed the same trend as polystyrene (where R_g is the radius of gyration of the polymer chain) (Roe, 2000). However, in the low-q region ($qR_g < 1$) the scattering was isotropic. The samples had segregated on crystallization, which is a well known problem with blends of deuterated and protonated polyethylene (Wignall, 1987). Hence, the anisotropy in the intermediate-q region came from structural factors rather than the chain conformation and mirrored that of the small-angle X-ray scattering (SAXS) data collected subsequently. While the calculated chain dimensions must be treated with some caution as a result of the segregation, they suggest that the deuterated molecules within the sample are actually isotropic. The aim of these experiments was to compare the results from other techniques with the original SANS experiments.

2. Experimental

The sample preparation and micro-injection molding of the thin plates and SANS experiments have been reported previously (Healy *et al.*, 2004). Flat plates of various thickness (dimensions $x = 14$ mm, $y = 0.31$, 0.70 and 1.0 mm, and $z = 26$ mm) were micro-injection molded using a Battenfeld Microsystem 50. A blend of 4 wt% deuterated linear polyethylene with a commercial grade linear polyethylene matrix was prepared in solution. The number average (M_n) and weight average (M_w) molecular weights for the matrix are M_n = 24 600 g mol^{-1} and M_w = 92 300 g mol^{-1}; and for the deuterated polymer they are M_n = 133 000 g mol^{-1} and M_w = 140 000 g mol^{-1}. During the injection molding process the part thickness and molding conditions, including the mold thickness and the injection speed, were systematically varied. The samples were sectioned to remove a 1 mm wide strip from the center of the sample to evaluate the change in morphology through the thickness of the part. Neutron scattering experiments were conducted on the 30 m SANS instrument on neutron guide NG7 at the National Institute of Standards and

Technology Centre for Neutron Research (NCNR, Gaithersburg, MD, USA) (Glinka *et al.*, 1998).

The SAXS data were collected at beamline 15ID-D ChemMatCARS, Advanced Photon Source (Argonne National Laboratory, Argonne, IL, USA) (Cookson *et al.*, 2006). The sample was mounted on a computer controlled sample changer on the SAXS/WAXS instrument and exposed to the X-ray beam of wavelength 1.1 Å for 1 s and 2 s. A Bruker 6000 charge-coupled device (CCD) detector was used to collect the SAXS data. The detector has a data collection area of 94 × 94 mm, with a pixel size of 92 × 92 µm. The detector was located symmetrically at a distance of 1.870 m from the sample position, enabling *d*-spacings in the range ~40 to 1100 Å to be studied. A 2 mm diameter beam stop located on a support arm protects the detector from the direct X-ray beam. The beam size was 500 × 500 µm for the beam parallel to the thickness direction (*y* axis) and 200 × 200 µm with the beam parallel to the sample width (*x* axis)

The wide-angle X-ray scattering (WAXS) data were collected at beamline 20B ANBF, Photon Factory (Tsukuba, Japan). The sample was exposed for 15 min in transmission mode using a wavelength of 1 Å and a beam size of 500 × 500 µm. The sample was exposed with the beam parallel to the thickness direction of the sample (along the sample *y* axis). Fuji image plates were used to collect the WAXS pattern with a camera length of 0.145 m. The crystalline peaks were separated from the amorphous scattering and the peak area was integrated in each case.

All samples were exposed with the beam perpendicular to the flow direction and either parallel or perpendicular to the surface of the flat plates. The background scattering intensity was collected for a sample-free configuration for the same exposure times and subtracted.

3. Results

Samples were exposed with the beam parallel to the thickness of the samples (along the sample *y* axis) and the beam illuminating the center of the plate (13 mm from the gate and 7 mm from the side shown in Fig. 1). Figs. 2–4 show the integrated peak intensity as a function of azimuth angle for the 200 and 020 reflections at various injection pin velocities and mold thicknesses. The measured intensity has been normalized for sample volume. The reference axis used is the flow (*z*) axis (azimuth angle of 0 and 180°).

A qualitative examination of the azimuth profiles shows that the 020 *b*-axis reflections from the crystallites have a preferential orientation perpendicular to the flow direction. The 200 *a*-axis reflections of the crystallites have a more complex profile with a much broader distribution that in some cases is clearly bimodal. This indicates the presence of two crystalline populations with a narrow peak perpendicular to the direction of flow (*z* axis) superimposed on the broad distribution preferentially aligned parallel to the flow direction.

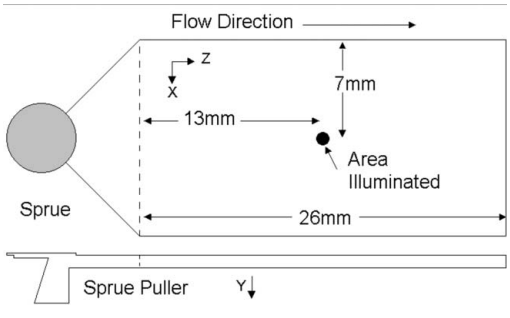

Figure 1
Injection molding showing the area illuminated for X-ray experiments.

The crystalline orientation can be quantified as a single value using Herman's orientation parameter *f* (Roe, 2000):

$$f = \tfrac{3}{2}\langle\cos^2\varphi\rangle - \tfrac{1}{2}, \tag{2}$$

where

$$\langle\cos^2\varphi\rangle = \frac{\int_0^{\pi} I(\varphi)\cos^2\varphi\sin\varphi\ \mathrm{d}\varphi}{\int_0^{\pi} I(\varphi)\sin(\varphi)\ \mathrm{d}\varphi} \tag{3}$$

and where φ is the angle between the crystalline reflection and the reference axis (the flow direction in this case). The value for *f* has been calculated for the 020 reflection (f_b); however, due to the complexity of the orientation of the 200 reflection a single parameter is not included here.

Table 1 shows comparative partial radii of gyration (R_{gx} and R_{gz}) determined using the Guinier approximation by taking sector integrals across and along the flow direction for the SANS data. Fig. 5 shows an example of a Guinier fit to the data. These data can be compared with f_b in Table 2 calculated for the *b* axis of the crystallites using the 020 peak. As Table 1 shows, the low-*q* region of the SANS data is close to isotropic for all the samples examined. On the other hand, the crystallites are strongly orientated for these polyethylene samples. The orientation of the crystallites decreases with increasing injection speed and the orientation was also increased for a given flow front speed by reducing the cavity thickness.

The corresponding SAXS data also show a decrease in lamellar orientation with increased injection velocity as shown in Fig. 6. The intensity was scanned for a *q* corresponding to the long spacing for the lamellar structure determined from the peak intensity of the Lorentz-corrected one-dimensional scattering profile.

The orientation of the *a* axis of the crystallites suggests that there is a mixture of crystalline growth mechanisms within the sample. Fig. 7 shows the SAXS patterns for material in the outer 200 µm of the sample and the core of the sample. The sample (0.15 m s^{-1} and 0.7 mm thick) is illuminated with a fine beam (200 × 200 µm) parallel to the *x* axis of the sample. Fig. 7a shows the presence of highly oriented row-nucleated structures evidenced by the equatorial streak perpendicular to the *z* axis showing the coherent scattering from the adjacent fibrils that function to nucleate the growth of highly oriented rows. These structures should produce lamellar growth (along the *b*

Table 1
SANS results for micro-injection molded polyethylene samples.

Injection speed (m s^{-1})	Mold thickness (mm)	R_{gx} (Å)	R_{gz} (Å)
0.15	0.31	454 ± 15	484 ± 57
0.15	0.70	383 ± 45	380 ± 45
0.15	1.0	346 ± 14	359 ± 21
0.75	0.31	394 ± 39	400 ± 21
0.75	0.70	383 ± 30	363 ± 29
0.75	1.0	374 ± 41	359 ± 27

Table 2
Herman's orientation parameter for micro-injection molded polyethylene samples.

Injection speed (m s^{-1})	Mold thickness (mm)	f_b
0.15	0.31	−0.392
0.15	0.70	−0.283
0.15	1.0	−0.132
0.75	0.31	−0.379
0.75	0.70	−0.228
0.75	1.0	−0.072

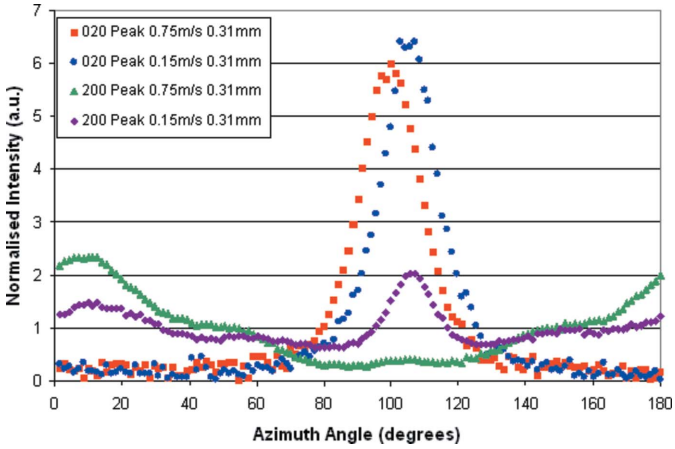

Figure 2
Integrated intensity of 200 and 020 peaks *versus* azimuth angle for the 0.31 mm thick mold.

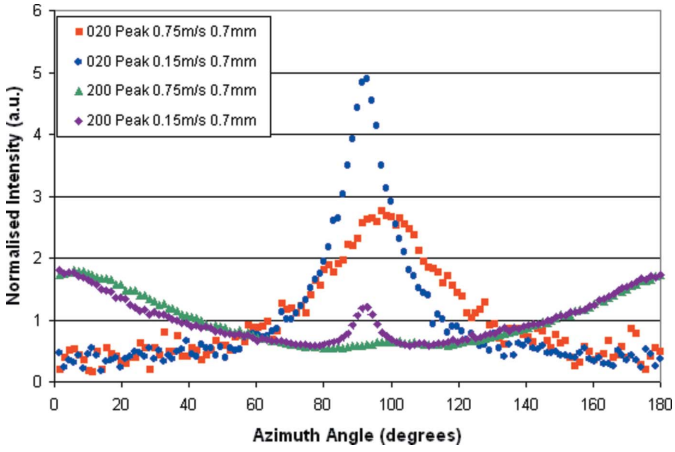

Figure 3
Integrated intensity of 200 and 020 peaks *versus* azimuth angle for the 0.70 mm thick mold.

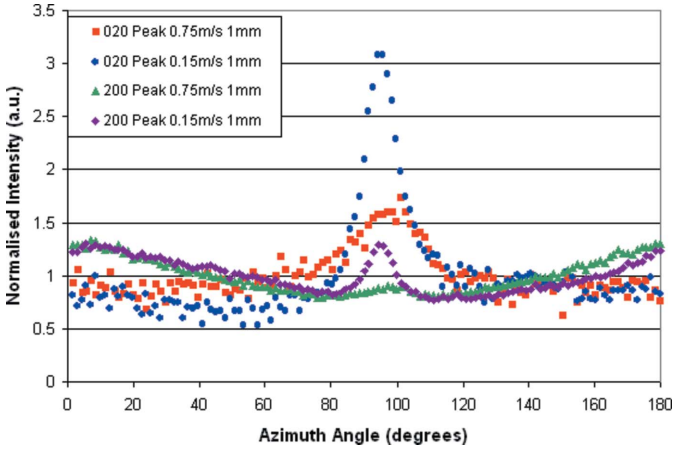

Figure 4
Integrated intensity of 200 and 020 peaks *versus* azimuth angle for the 1.0 mm thick mold.

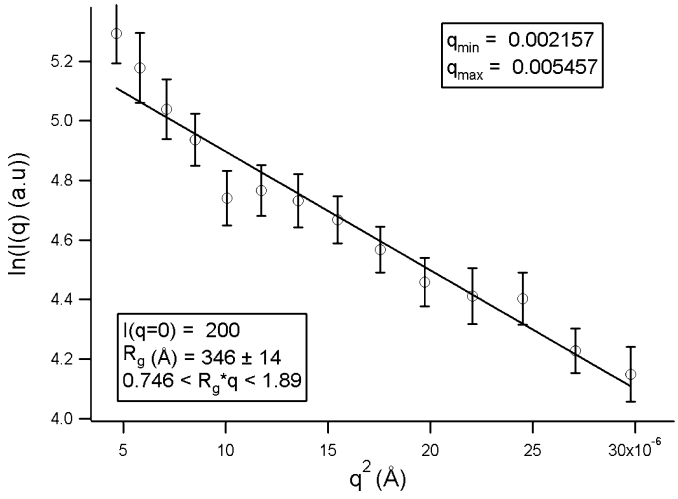

Figure 5
Example of a Guinier fit for 0.15 m s^{-1} 1 mm mold.

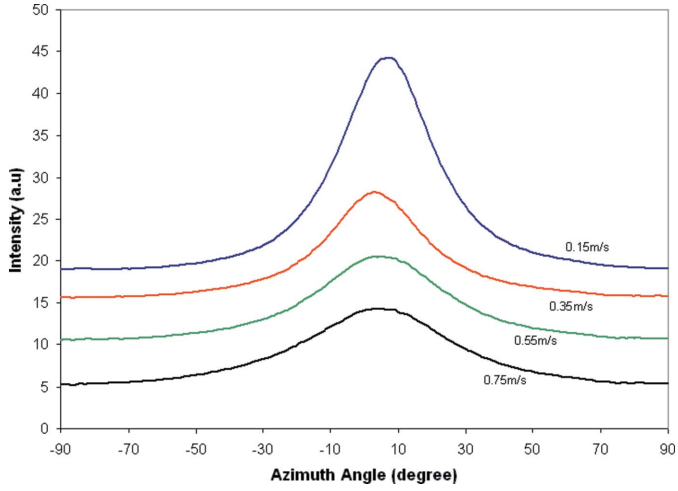

Figure 6
Intensity *versus* azimuth angle for the 0.7 mm thick mold and various injection velocities. Curves have been progressively offset by 5 arbitrary units along the *y* axis with decreasing injection velocity.

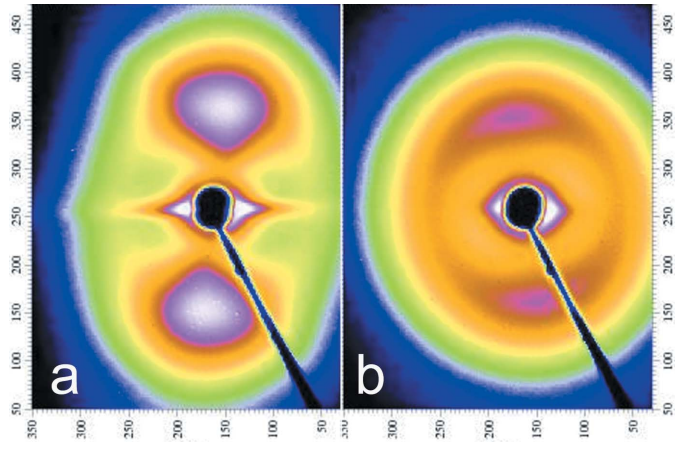

Figure 7
SAXS patterns showing the variation in morphology through the thickness of the sample (sample 0.15 m s^{-1}, 0.7 mm). The flow direction is vertical; Fig. 7a is the outer 200 µm while Fig. 7b is from the core of the sample. *z* (vertical) and *y* scales are in pixels.

axis) perpendicular to the direction of applied shear (Katti & Schultz, 1982).

4. Discussion

These polyethylene samples showed minimal anisotropy in the low-q region of the SANS data. However, the data are not entirely unambiguous due to the observed excess scattering caused by segregation of the protonated and deuterated chains. The SANS data only measure the orientation of the deuterated chains within the sample, while the WAXS/SAXS data measure the average orientation of the crystallites of the entire sample. The absence of orientation in the SANS data does not exclude chain orientation within the sample for chains of different length than those used. However, if it is assumed that chains of shorter length than the deuterated chains are similarly unoriented it suggests that the bulk of the polymer chains are relaxed prior to crystallization. This seems to suggest that the majority of the residual orientation of the crystallites is driven by oriented crystal growth rather than initial chain orientation.

While the orientation of the b axis of the crystallites is consistently aligned perpendicular to the flow direction, the a-axis orientation is more complex, suggesting a mixture of crystalline growth mechanisms. As the SAXS data show, 'shish-kebab' type row-nucleated structures are present at low injection speeds near the surface (Fig. 7a). Near the center of the sample the lamellar scattering is still preferentially aligned (though less so) along the direction of flow but there is no evidence of the shish fibrils in the equatorial scattering as observed in the scattering from material in the outer layer (Fig. 7b). Keller & Kolnaar (1993) proposed that under high shear (such as near the surface of the mold) the level of row nucleation is high and the lamellar growth will be perpendicular to the fibril orientation giving both a- and b-axis orientation perpendicular to the direction of the applied shear. At lower shear rates (such as at the center of the mold) the number of nucleating fibrils is reduced and the growing lamellar are able to twist around the growth (b) axis producing an a-axis orientation parallel to the direction of applied shear.

Pople *et al.* (1996) observed the oriented crystal growth in a polymer melt that had returned to a quiescent state after shear flow. Pople *et al.* (1996) proposed that very long chains in the polymer melt retain their orientation over long periods and act as row-nucleating structures for the shorter chains that make up the bulk of the polymer even once the bulk of the polymer chains have relaxed. It has been shown experimentally that epitaxically oriented crystal growth can occur in a quiescent polymer melt if appropriate nucleating structures are added (Gu *et al.*, 2000). Hence, it is unnecessary for polymer chains to be oriented in order to engage in oriented crystal growth and it is possible that for the bulk of the polymer sample the overall chain orientation remains unperturbed during crystallization.

Yu & Wilkes (1996) provided further experimental support for the idea that it is the very long chains within a polymer matrix that are responsible for the formation of the fibrils responsible for row nucleation. They found that increasing the number of long chains induced a row-nucleated structure in extruded tubular films. Yu & Wilkes (1996) also found that while there was considerable crystalline anisotropy there was minimal thermal shrinkage of the part along the orientation direction on heating. This indicates that the material had limited chain orientation and is consistent with the conclusions drawn here.

The segregation effect is unfortunate but it is difficult to see how this can be eliminated altogether using polyethylene. Even novel approaches such as that by Crist & Nicholson (1993) have not succeeded in eliminating the problem for polyethylene. The study could be repeated using another semi-crystalline polymer; however, this will obviously change the crystallization kinetics and chain relaxation rate.

5. Conclusions

Processing of semi-crystalline polymers through injection micromolding can produce moldings with substantial residual orientation. These data suggest that the primary source of orientation in injection molded semi-crystalline polymers is crystal growth oriented by row-nucleating structures formed during polymer processing rather than chain orientation of the bulk of the sample produced by the flowing polymer melt. These data are consistent with a model for oriented crystal growth that does not require any pre-orientation of the polymer chains other than the initial nucleating structures.

Use of the Australian National Beamline Facility (ANBF) and of the ChemMatCARS Sector 15 at the Advanced Photon Source was supported by the Australian Synchrotron Research Program, which is funded by the Commonwealth of Australia under the Major National Research Facilities Program. ChemMatCARS Sector 15 is principally supported by the National Science Foundation/Department of Energy under grant No. CHE-0535644. Use of the Advanced Photon Source was supported by the US Department of Energy, Office of Science, Office of Basic Energy Sciences, under contract No. DE-AC02-06CH11357. We acknowledge the support of the National Institute of Standards and Technology, US Department of Commerce, in providing the neutron research facilities used in this work. This work was supported by the CRC for Polymers and AINSE. The injection molding was performed at the University of Bradford and the authors would like to thank Dr Ben Whiteside for his invaluable assistance and patience.

References

Cookson, D., Kirby, N., Knott, R., Lee, M. & Schultz, D. (2006). *J. Synchrotron Rad.* **13**, 440–444.
Crist, B. & Nicholson, J. C. (1993). *Polymer*, **35**, 1846–1854.
Glinka, C. J., Barker, J. G., Hammouda, B., Krueger, S., Moyer, J. J. & Orts, W. J. (1998). *J. Appl. Cryst.* **31**, 430–445.
Gu, F., Bu, H. & Zhang, Z. (2000). *Macromolecules*, **33**, 5490–5494.
Healy, J., Edward, G. H. & Knott, R. B. (2004). *Proceedings of the Annual Technical Conference of the Society of Plastics Engineers (ANTEC)*, pp. 3433–3436. Brookfield, CT: Society of Plastics Engineers.
Ito, H., Yagisawa, Y., Saito, T., Yashuhara, T., Kikutani, T. & Yamigiwa, Y. (2005). *Proceedings of the Annual Technical Conference of the Society of Plastics Engineers (ANTEC)*, pp. 894–898. Brookfield, CT: Society of Plastics Engineers.
Katti, S. S. & Schultz, J. M. (1982). *Polym. Eng. Sci.* **22**, 1001–1017.
Keller, A. & Kolnaar, J. W. H. (1993). *Prog. Colloid Polym. Sci.* **92**, 81–102.
Pople, J. A., Mitchell, G. R. & Chai, C. K. (1996). *Polymer*, **37**, 4187–4191.
Roe, R.-J. (2000). *Methods of X-Ray and Neutron Scattering in Polymer Science*, pp. 123–125. New York: Oxford University Press.
Wignall, G. D. (1987). *Neutron Scattering. Encyclopedia of Polymer Science and Engineering*, Vol. 10, pp. 112–184. New York: John Wiley.
Yu, T.-H. & Wilkes, G. L. (1996). *Polymer*, **37**, 4675–4687.